IEEE Open Journal of
Antennas and Propagation

Received 17 August 2023; revised 14 September 2023; accepted 22 September 2023. Date of publication 27 September 2023;
date of current version 16 October 2023.

Digital Object Identifier 10.1109/OJAP.2023.3319631

Compact and Broadband Substrate Integrated Dielectric Resonator Antenna Suitable for 5G Millimeter-Wave Communications

JIE-ER ZHANG [1], QINFANG ZHANG [1], WEI QIN [2] (Member, IEEE), WEN-WEN YANG [2] (Member, IEEE), AND JIAN-XIN CHEN [2] (Senior Member, IEEE)

[1]School of Materials Science and Engineering, Yancheng Institute of Technology, Yancheng 224051, China

[2]School of Information Science and Technology, Nantong University, Nantong 226019, China

CORRESPONDING AUTHOR: W.-W. YANG (e-mail: wwyang2008@hotmail.com)

This work was supported in part by the National Natural Science Foundation of China under Grant 62071256; in part by the Qing Lan Project of Jiangsu Province; and in part by the Nantong Research Institute for Advanced Communication Technologies.

ABSTRACT To date, few broadband DRAs can cover n257, n258, n260, and n261 bands with a small physical footprint (e.g., < $0.4\lambda_0 \times 0.4\lambda_0 \times 0.15\lambda_0$, where λ_0 is the free-space wavelength at 28GHz). This article proposes a compact and broadband substrate-integrated dielectric resonator antenna (SIDRA) suitable for 5G millimeter-wave band applications. Four operating modes from three resonators, including TE_{111} and TE_{131} modes from the DR, slot mode from the H-shaped feeding slot, and patch mode from the inserted ring patch, are excited to achieve a bandwidth of 61.9% (24-45.5 GHz) with a compact size of $0.37\lambda_0 \times 0.37\lambda_0 \times 0.125\lambda_0$. The proposed DRA can be extended to an array with ~0.5 λ_0 element interval to obtain wide-angle beam scanning capability. A 1×4 SIDRA array was simulated, achieving beam-scanning area of ±45° and ±32° at the frequencies of 28 / 39 GHz. Further, the DRA array was fabricated and tested. It offers a measured 10-dB bandwidth ($|S_{11}| \leq -10$ dB) of ~60.4% (23.5-43.7 GHz), in which the gain varies between 10.1 to 12.5 dBi.

INDEX TERMS Broadband, compact, dielectric resonator antenna, millimeter-wave, beam-scanning.

I. INTRODUCTION

IN RECENT years, millimeter-wave antennas are widely used to provide high-data-rate communications in fifth-generation (5G) technologies [1], [2]. Generally, millimeter-wave antennas should be designed based on the following considerations: **1) Wide bandwidth.** Several commercial bands in millimeter-wave region are introduced, such as n257, n258, n260, n261, etc., ranging from 24.25 to 43.5 GHz. The antennas which can cover the whole bandwidth would become very attractive. **2) Compact size.** To achieve wide angular coverage and avoid grating lobes, the element spacing of beam-scanning arrays are required to be around 0.5 λ_0 (λ_0 is the free-space wavelength at 28GHz) [3], [4]. Therefore, the antenna element should be compact enough (<$0.4\lambda_0 \times 0.4\lambda_0$) to support the array design requirements. **3) High efficiency.** The adoption of massive multiple-input multiple-output (Massive-MIMO) technology in millimeter-wave bands results in a significant rise in energy consumption. To improve energy efficiency, it is essential for the antenna to possess high antenna efficiency.

Several types of millimeter-wave antennas have been proposed to cover the target bands in recent years. One method is to use stacked patches [5], [6], [7], [8], [9], [10], [11]. In [7], a dual-polarized antenna is proposed with two layers of gridded patches. In [9], the presented antenna has a stacked patch configuration with extra parasitic strips. However, most of these designs can only support dual-band operation. To fully cover the frequency band between 24 to 43 GHz, magneto-electric (ME) dipoles [12], [13], [14], [15], [16] and so-called complementary antennas [17], [18] are proposed. In [16], by combining the patches (electric dipole) and a via-slot structure (magnetic dipole), the antenna achieves a bandwidth of 24.3-40 GHz. In [17], the complementary design can cover the bandwidth of 27–45.5 GHz.

It is noted that all the aforementioned antennas are metallic antennas, which suffer from the defect of high ohmic losses in the millimeter-wave band, therefore having relatively low efficiency. To solve this issue, dielectric resonator antenna (DRA), which has higher antenna efficiency, is considered as a promising candidate [19], [20], [21], [22], [23], [24], [25], [26], [27], [28], [29], [30], [31], [32]. In [20], a 2×2 DRA array can achieve a bandwidth of 25-40 GHz by using a novel but bulky feeding structure. In [26], a low profile and decoupled connected DRA array is presented. However, it can only cover a bandwidth of 22.5-30 GHz. To the authors' knowledge, there is currently no reported DRA design that can provide a wide bandwidth spanning from 24 GHz to 43 GHz, while maintaining a compact size suitable for wide-angle beam-scanning applications.

To solve this issue, a compact and broadband substrate-integrated DRA (SIDRA) is proposed in this article. Compared to ceramic DRA, SIDRA is more convenient for processing and assembly [33], [34]. By properly combining the DR, slot, and ring patch, the proposed antenna can produce a total of four resonant modes. Specifically, the fundamental mode TE_{111} and higher order mode TE_{131} of the DRA are excited at 32 GHz and 43.5 GHz, respectively. The H-shape slot feeding structure also functions as a resonant radiator at 25 GHz, whereas the ring patch produces an additional mode at around 38 GHz. The antenna can, therefore, cover the whole millimeter-wave band of 24-43 GHz with a small physical footprint of 0.37 λ_0×0.37 λ_0×0.125 λ_0. It can also be extended to an array with ∼0.5 λ_0 element interval to obtain wide-angle beam scanning capability.

II. MULTI-MODE HYBRID DRA

A. ANTENNA CONFIGURATION

Fig. 1 illustrates the configuration of the proposed SIDRA. It is a PCB-based multilayered structure containing three substrate layers and two prepreg layers. The square SIDRA is directly constructed in Substrate 1, having a side length of a. A square-ring patch is printed on the upper surface of Substrate 2, whose outer length is given by a_m and inner length by a_n. An H-shaped slot is etched on the upper metallic layer of Substrate 3, while an microstrip line is printed on the bottom surface. They together server as a feeding structure to excite the above SIDRA.

In this case, Substrate 1 is made of Taconic RF-10 ($\varepsilon_{r1} = 10.2$, $tan\delta = 0.0025$) with a thickness of h_1. Taconic RF-35 ($\varepsilon_{r2} = 3.5$, $tan\delta = 0.0018$) with a thickness of h_2 and Rogers 5880 ($\varepsilon_{r3} = 2.2$, $tan\delta = 0.0009$) with a thickness of h_3 are used for Substrate 2 and Substrate 3, respectively. The three substrates are pressed together by using two prepreg layers (thickness is h_{preg}) of Rogers 4450F ($\varepsilon_{r4} = 3.54$, $tan\delta = 0.004$).

B. OPERATING PRINCIPLE

To investigate the operation of the proposed SIDRA, the evolution of the antenna structure is studied. Fig. 2 shows the configurations of the three antennas, while Fig. 3 depicts

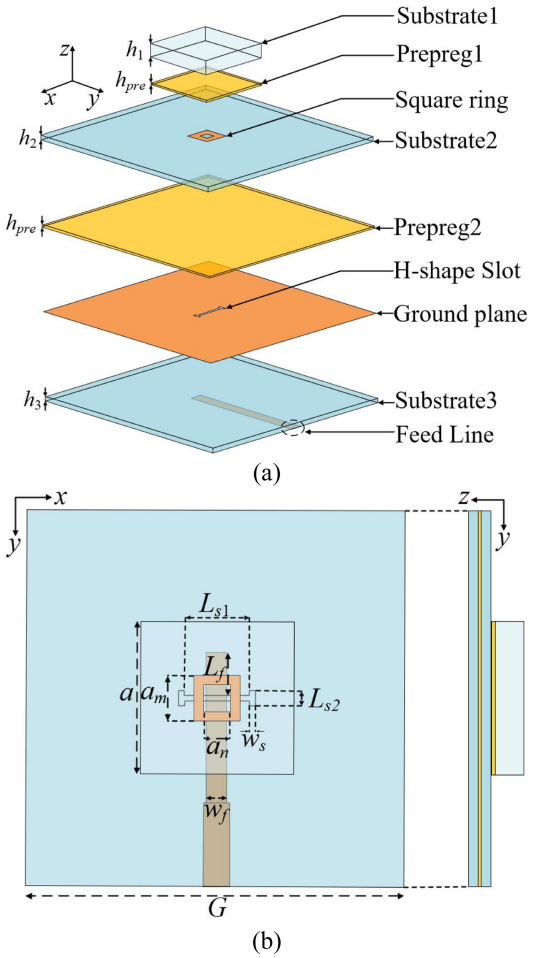

FIGURE 1. ConFiguration of the proposed SIDRA. $h_1 = 0.635$ mm, $h_2 = 0.254$ mm, $h_3 = 0.254$ mm, $h_{pre} = 0.1$ mm, a = 4 mm, $a_m = 0.8$ mm, $a_n = 0.7$ mm, $L_{s1} = 1.7$ mm, $L_{s2} = 0.4$ mm, $L_f = 1.13$ mm, $w_s = 0.15$ mm, $w_f = 0.6$ mm, $G = 12$ mm.

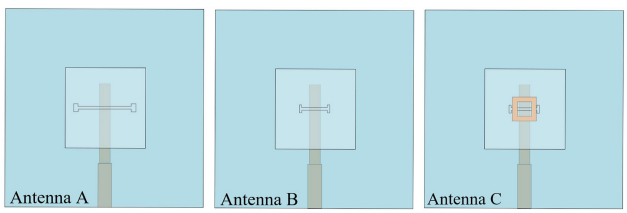

FIGURE 2. Structure evolution of the proposed SIDRAs.

the corresponding simulated reflection coefficients. The full-wave solver ANYSIS HFSS is used for simulation. It is found that antenna A have two resonances at 31 GHz and 44 GHz, which is contributed by the DRA's fundamental TE_{111} mode and the high-order TE_{131} mode, respectively. To include the feeding slot mode, Antenna B is achieved by adjusting the size of the H-shaped slot, mainly shortening its length. Through the adjustment, the slot mode is shifted up to around 25 GHz, which is close to the TE_{111} mode and the bandwidth has potential to be enhanced. However, even though the three resonant modes are excited within the target band, it is difficult to optimize the impedance

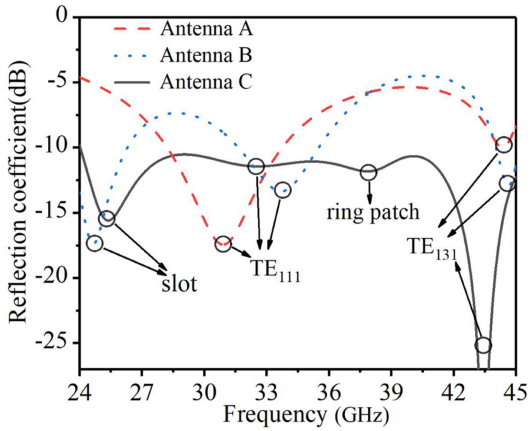

FIGURE 3. Simulated $|S_{11}|$s for the antennas with different structures.

matching since the two resonances from the DRA are still too far apart. To solve this issue, a square ring patch is introduced in Antenna C. It produces an additional mode at 38 GHz which is located right between the DRA's two resonances. With this operation, four resonances can be created and uniformly distributed over the target frequency band, and a good impedance matching within the band can finally be achieved for Antenna C. Here it is important to note that the adopted ring patch has two advantages. First, it has a very small size (much smaller than a square patch), thus having little influence on the other resonators. Second, it does not increase the overall antenna dimension as it is inserted below the DRA.

To further investigate the operation mechanism of the SIDRA, the E-field patterns of the antenna at different resonant frequencies in the *xoy* and *yoz* planes are illustrated in Fig. 4. Fig. 4(a) depicts the E-field patterns at 25 GHz, which can be seen that a strong E-field distribution is concentrated around the H-shaped slot, suggesting that the resonance is generated by the slot. In Fig. 4(b) and Fig. 4(d), it can be found that the E-field distribution is concentrated on the upper surface of the DRA at 32 GHz and 43.5 GHz, and the corresponding shapes of the field pattern are consistent with the DRA's fundamental TE_{111} mode and higher-order TE_{131} mode. Fig. 4(c) shows the E-field distributions at 38GHz. It is quite strong around the ring patch. On this basis, the mode around 38 GHz can be defined as a ring patch mode.

C. PARAMETRIC STUDIES

In order to provide a clear demonstration of how the different structural parameters affect the antenna, parametric studies have been performed. Fig. 5(a) shows the simulated $|S_{11}|$ corresponding to different lengths (L_{s1}) of the H-shaped slot. With reference to the figure, the first resonant mode decreases from 26 GHz to 23.5 GHz as L_{s1} increases from 1.5 to 1.9 mm while the other resonances remain stable. This phenomenon also indicates that the resonance around 25 GHz is closely related to the H-shaped slot.

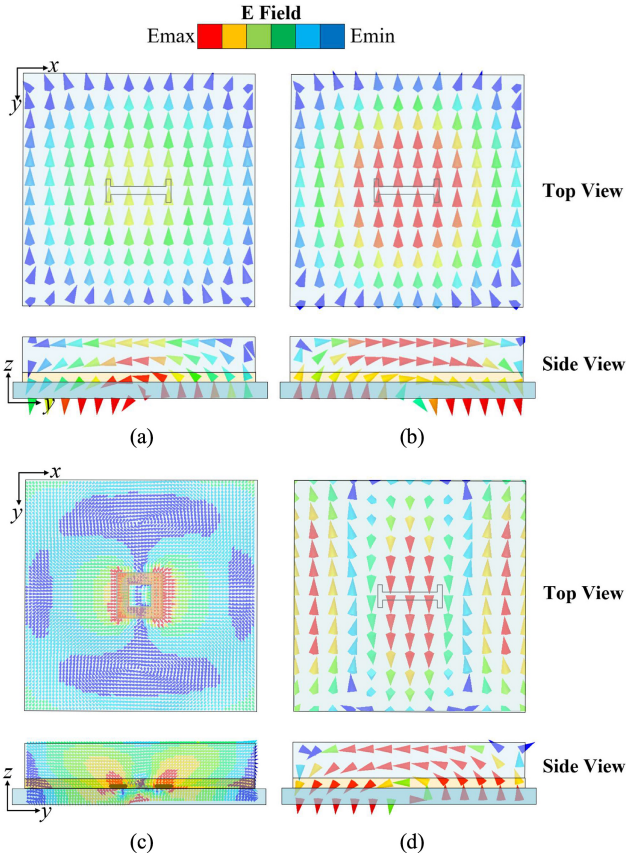

FIGURE 4. Simulated E-field patterns of the SIDRA. (a) Slot mode at 25 GHz. (b) TE_{111} mode at 32 GHz. (c) Ring patch mode at 38 GHz. (d) TE_{131} mode at 43.5 GHz.

The impact of the DR on the antenna was also investigated. The reflection coefficients against a and h_1 are simulated in Fig. 5(b) and (c). As a and h_1 increase, the resonant frequencies around 32 GHz (TE_{111} mode) and 43.5 GHz (TE_{131} mode) shift downward apparently as the other two resonances remain unchanged. This is reasonable because both the second and fourth modes are produced by the DRA. It is worth noting that the influence of a on the resonance of TE_{131} mode is slightly stronger than that on TE_{111} mode, while h_1 has the opposite influence on the two resonances.

A parametric study of the side length of ring patch was carried out in Fig. 5(d). It can be learned that the variation of a_m significantly affects the resonant frequency around 38 GHz. This phenomenon confirms that the third resonant mode is mainly generated by the ring patch.

D. DESIGN GUIDELINE

Based on the operating principle mentioned above, a concise design guideline is summarized as follows:

1. *Determining the dimensions of the square SIDRA.* The initial values of the SIDRA is determined to ensure the resonances of TE_{111} and TE_{131} modes radiate at target frequencies.
2. *Inserting the ring patch to extend the bandwidth.* The small ring patch has negligible effect on the DR

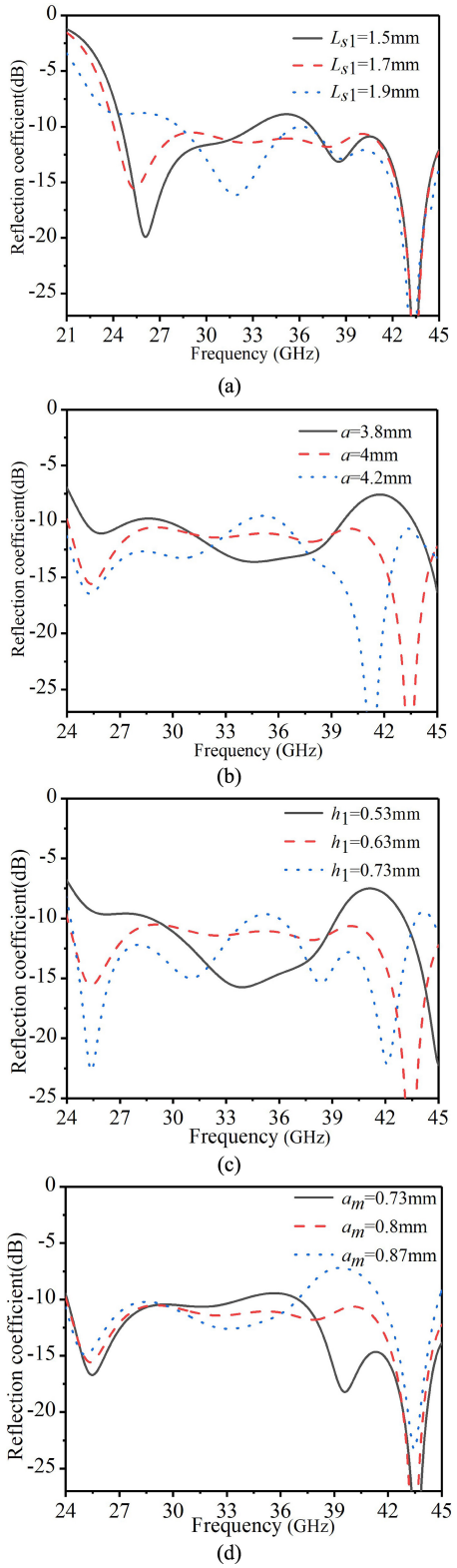

FIGURE 5. Simulated $|S_{11}|$s of the antenna with different (a) L_{s1} (b) a (c) h_1 (d) a_m.

operation. It can be then inserted into the DRA with its size determined to enhance the antenna bandwidth.

3. *Tuning the length of slot.* In addition to tuning the impedance matching, the H-shaped slot is also operating as a resonator. The slot size should be carefully tuned for both the mode resonating and impedance matching.
4. *Optimizing the antenna structure.* The parameters of antenna can be further optimized to achieve a good performance.

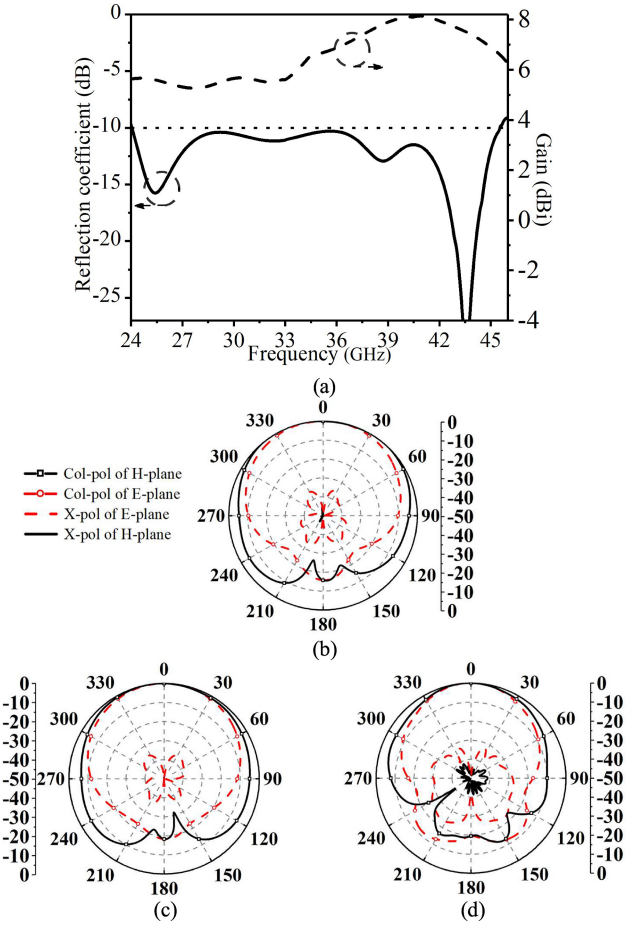

FIGURE 6. Simulated $|S_{11}|$, gain and radiation patterns at different frequencies of the SIDRA element. (a) $|S_{11}|$ and gain. (b) 26 GHz patterns. (c) 32 GHz patterns. (d) 38 GHz patterns.

E. SIMULATED RESULTS OF THE SIDRA ELEMENT

Fig. 6 depicts the simulated performance of the DRA element. The reflection coefficient and gain are shown in Fig. 6(a). With reference to the figure, the impedance bandwidth ($|S_{11}| < -10$ dB) is given by 61.9% (24-45.5 GHz), and the gain is stable between 5.3 dBi and 8.1 dBi within the impedance bandwidth.

The radiation patterns at low (26 GHz), middle (32 GHz), and high (38 GHz) frequencies are presented in Fig. 6(b)-(d). The simulated results demonstrate that the antenna element can achieve symmetrical radiation patterns on both the planes across the wide operating band. Within the 3-dB beamwidths, the cx-pol (cross-polarization) levels remain below –32 dB in the E-plane and –41 dB in the H-plane.

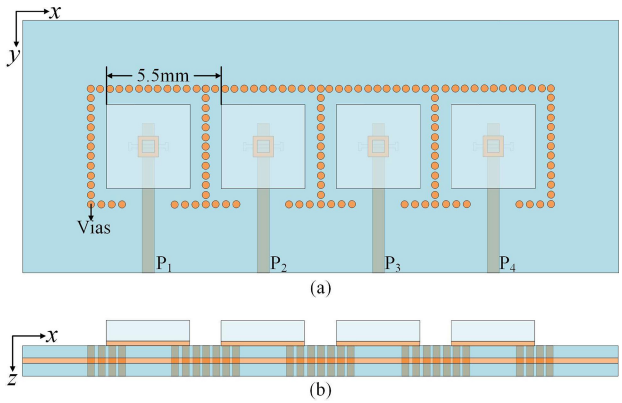

FIGURE 7. Structures of the proposed SIDRA array. (a) Top view. (b) Side view.

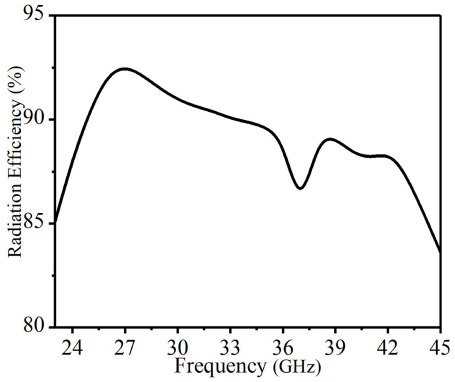

FIGURE 8. Simulated radiation efficiency of the proposed antenna array.

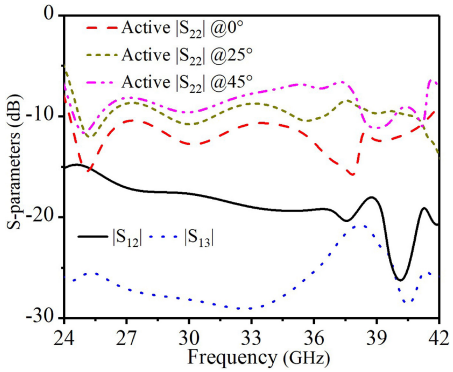

FIGURE 9. Simulated active S-parameters and mutual couplings between the ports of the antenna array.

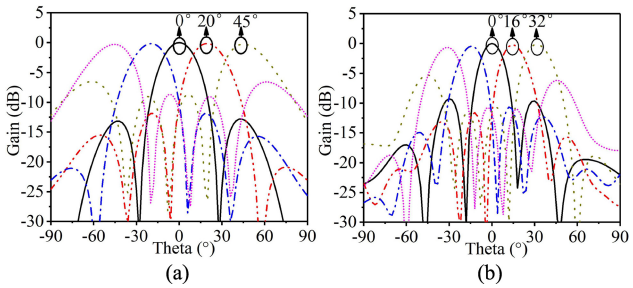

FIGURE 10. 2-D beam-scanning results of the SIDRA array at different frequencies. (a) 28 GHz. (b) 39 GHz.

III. 1×4 HYBRID ANTENNA ARRAY

The proposed SIDRA is extended to a 1×4 array as shown in Fig. 7 since a 1×4 array is currently the most commonly used millimeter-wave antenna solution for mobile terminals. To achieve a wide-angle coverage, the element spacing is set as 5.5mm (~$0.51\lambda_0$ at 28 GHz). The plated-through-vias surrounding the antenna elements are used to reduce the mutual coupling. Fig. 8 shows the simulated radiation efficiency of the proposed antenna array, which is varying from 83.6% to 92.5%.

Fig. 9 shows the simulated active $|S_{22}|$s and mutual couplings between different ports of the antenna array, where we can learn that the mutual coupling is lower than –15 dB within the band. The active parameters are better than –10 dB at the scanning angle of 0° (@28 GHz) and better than –8.5 dB with the scanning area of ±25°. When scanning angle increases up to 45°, the active $|S_{22}|$ is better than –6.5 dB.

Fig. 10 illustrates the simulated 2D beam-scanning performance of the DRA array by introducing a stepwise phase shift between the elements at 28 / 39 GHz. In H-plane, the observed scan losses are lower than 1 dB with sidelobe levels better than 5 dB within the scanning area of ±45° and ±32° at 28 GHz and 39 GHz.

The proposed design concepts were verified by fabricating and measuring the antenna array. Fig. 11 (a) and (b) show the antenna prototype, where we can find that a one-to-four Wilkinson power divider is introduced to do the measurement of the radiation patterns at 0° scanning angle. Fig. 11(c) demonstrates the corresponding measured and simulated antenna performance of gains and $|S_{11}|$s. The simulated –10 dB impedance bandwidth is 61.7% (23.2–43.9 GHz) and the measured one is 60.4% (23.5–43.7 GHz). The simulated gain varies from 10.8 dBi to 13.5 dBi, and the measured array gain varies between 10.1 dBi and 12.5 dBi.

Fig. 12 illustrates the radiation patterns of the SIDRA array, showing both simulated and measured results. The measured main lobes match well with the simulated ones at all three frequencies. In the H-plane, the measured maximum sidelobe levels are given by –12.5 dB, –12.4 dB, and –16.7 dB. The measured X-pol levels within the 3-dB beamwidths are better than –29.2 dB/–25.2 dB/–29.7 dB in the E-plane and –29 dB/–27.4 dB/–27 dB in the H-plane at 26/32/38 GHz, respectively. Suffer from the fabrication tolerances as well as the measurement error, there are some slight discrepancies between the simulated and measured results.

Table 1 presents a comparative analysis between the proposed SIDRA and previously reported millimeter-wave DRAs, highlighting the contributions of this paper. It can be found that majority of the DRA designs have limited bandwidths and cannot achieve the full band coverage of 24.25-43.5 GHz. In [20], although the DRA obtains a wide bandwidth of 42% (covering 25-40 GHz), it has

TABLE 1. Performance comparison with the previous antenna designs.

Ref	SIDRA	Number of modes	Array scale	Im. BW (GHz)	Element Gain (dBi)	Array Gain (dBi)	**Radiation Efficiency (%)**	Beam-scanning capability	Maximum Beam-Scanning Angle	Element Size*
[19]	No	2	-	27.7-32.7 (16.6%)	10.5-11.3	-	**-**	No	-	$1.31\times1.31\times1.19(\lambda_0^3)$
[20]	No	3	2×2	25-40 (42%)	5.3-7.4	7-10.5	**>90**	No	-	$0.43\times0.43\times0.33(\lambda_0^3)$
[23]	Yes	3	1×4	29.6-33.2 (11.5%)	5-7.85	5.9-9.8	**-**	No	±45°@31 GHz	$0.26\times0.45\times0.08(\lambda_0^3)$
[24]	Yes	3	1×4	25.3-31.5 (21.8%)	~6.38	~13	**-**	Yes	~±40°@28 GHz	$0.43\times0.43\times0.11(\lambda_0^3)$
[25]	No	3	1×4	23.6–31 (27.1%)	-	9.2-10.5	**>89.6**	Yes	±40°@27 GHz	$0.31\times0.49\times0.07(\lambda_0^3)$
[26]	No	3	1×4	23.2-30.5 (27.2%)	-	10.2-11.3	**85.5-92**	No	-	$0.3\times0.45\times0.1(\lambda_0^3)$
[27]	No	4	1×5	26.4-30.1(13.1%) 36.4-40.5(11%)	<7.3 <7.1	<12.6 <13.8		Yes	±50°@28 GHz ±40°@39 GHz	$0.34\times0.36\times0.10(\lambda_0^3)$
[28]	Yes	2	4×4	62.7-73.9 (16.4%)	-	6-17	**89.2**	No	-	$0.4\times0.4\times0.2(\lambda_1^3)$
[29]	No	4	-	12.2-27.1 (75.8%)	0.3-6.4	-	**-**	No	-	$0.33\times0.87\times0.24(\lambda_2^3)$
[30]	Yes	-	4×4	48.5-66 (30.6%)	6.3-7	15-17.5	**-**	No	-	$0.21\times0.21\times0.3\ (\lambda_3^3)$
[31]	No	1	1×4	58-62 (7%)	~5	9-10.6	**87-91**	No	-	$0.2\times0.2\times0.1(\lambda_4^3)$
[32]	Yes	2	4×4	50.27-70 (33%)	5-7.5	15.5-17	**>83**	No	-	$0.29\times0.29\times0.2(\lambda_4^3)$
Prop.	Yes	4	1×4	24-45.5 (61.9%)	5.3-8.1	10.8-13.5	**83.6-92.5**	Yes	±45°@28 GHz ±32°@38 GHz	$0.37\times0.37\times0.125(\lambda_0^3)$

* λ_0/ λ_1/ λ_2/ λ_3 /λ_4 means the free-space wavelength @28 GHz/67 GHz/20 GHz/56 GHz/58 GHz.

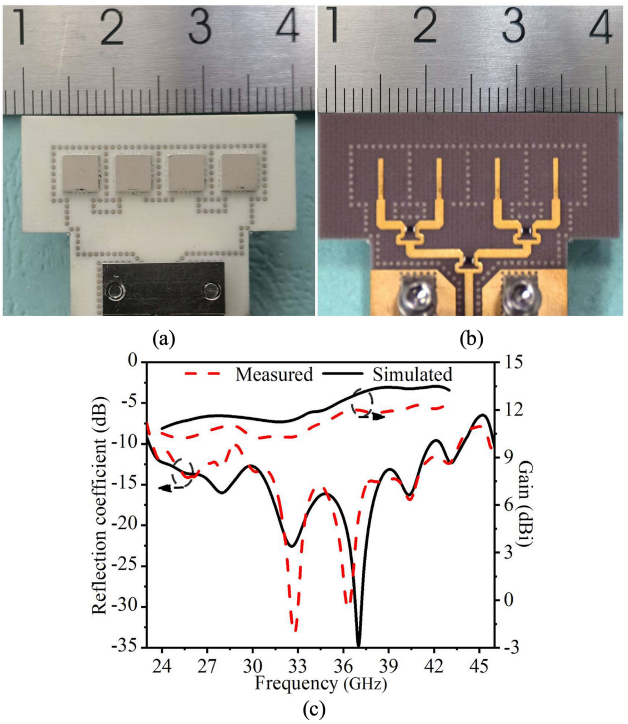

FIGURE 11. The prototype of the 1×4 DRA array with its measured and simulated results. (a) Top view of the array prototype. (b) Bottom view of the array prototype. (c) Measured and simulated gains and $|S_{11}|$s of the array prototype.

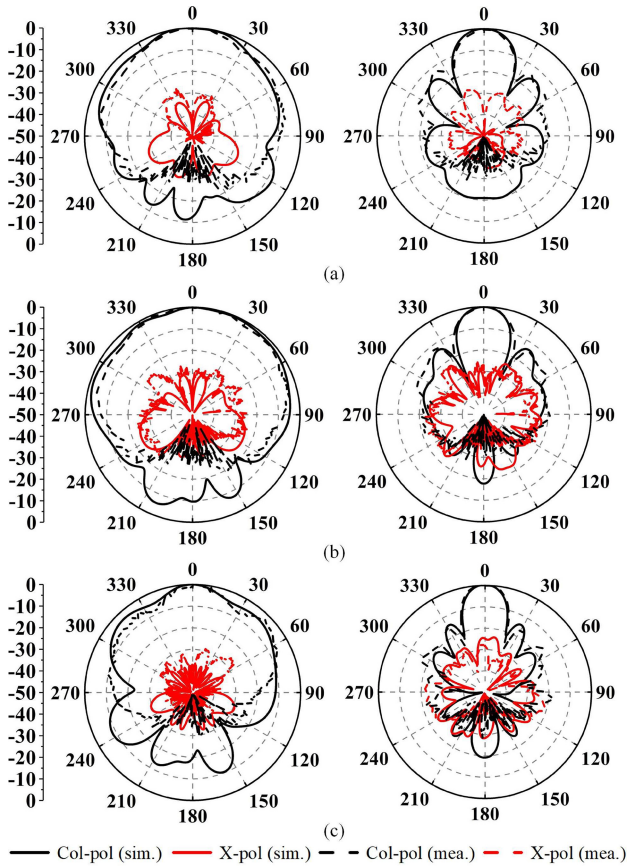

FIGURE 12. Simulated and measured radiation patterns of the SIDRA array at (a) 26 GHz. (b) 32 GHz. (c) 39 GHz.

a complicated feed structure which makes it hard to be extended to an array design. The proposed SIDRA element has comparable compact size and radiation efficiency with the competitors, but demonstrating a much wider bandwidth. Furthermore, the proposed antenna can be extended to an array to support wide-angle beam scanning. Moreover, it can be fabricated by using standard PCB process, which can mitigate the positioning error and improve the integration level, enabling the applications in commercialized batch fabrication at millimeter-wave band.

IV. CONCLUSION

In this article, a compact and broadband SIDRA and its array design have been constructed and investigated for 5G millimeter-wave applications. A wide bandwidth, which can cover the whole n257, n258, n260 and n261

(24.25-43.5 GHz) bands, has been realized by exciting four different operating modes. Within the bandwidth, the SIDRA can also achieve stable radiation patterns and gain. The proposed SIDRA element has been further extended to a 1×4 antenna array. The simulated results reveal that the array can achieve wide beam-scanning angles at target frequencies. The measured $|S_{11}|$s, gains and radiation patterns show tolerable differences compared to the simulated results. It can be concluded that the proposed design is valuable for millimeter-wave applications.

REFERENCES

[1] N. Bhushan et al., "Network densification: The dominant theme for wireless evolution into 5G," *IEEE Commun. Mag.*, vol. 52, no. 2, pp. 82–89, Feb. 2014.

[2] W. Hong, K. Baek, and S. Ko, "Millimeter-wave 5G antennas for smartphones: Overview and experimental demonstration," *IEEE Trans. Antennas Propag.*, vol. 65, no. 12, pp. 6250–6261, Dec. 2017.

[3] Y. Huo, X. Dong, and W. Xu, "5G cellular user equipment: From theory to practical hardware design," *IEEE Access*, vol. 5, pp. 13992–14010, 2017.

[4] W. Roh et al., "Millimeter-wave beamforming as an enabling technology for 5G cellular communications: Theoretical feasibility and prototype results," *IEEE Commun. Mag.*, vol. 52, no. 2, pp. 106–113, Feb. 2014.

[5] J. Chen, M. Berg, K. Rasilainen, Z. Siddiqui, M. E. Leinonen, and A. Pärssinen, "Broadband cross-slotted patch antenna for 5G millimeter-wave applications based on characteristic mode analysis," *IEEE Trans. Antennas Propag.*, vol. 70, no. 12, pp. 11277–11292, Dec. 2022.

[6] Z. Siddiqui et al., "Dual-band dual-polarized planar antenna for 5G millimeter-wave antenna-in-package applications," *IEEE Trans. Antennas Propag.*, vol. 71, no. 4, pp. 2908–2921, Apr. 2023.

[7] W. Sun, Y. Li, L. Chang, H. Li, X. Qin, and H. Wang, "Dual-band dual-polarized microstrip antenna array using double-layer gridded patches for 5G millimeter-wave applications," *IEEE Trans. Antennas Propag.*, vol. 69, no. 10, pp. 6489–6499, Oct. 2021.

[8] X. Tong, Z. H. Jiang, C. Yu, F. Wu, X. Xu, and W. Hong, "Low-profile, broadband, dual-linearly polarized, and wide-angle millimeter-wave antenna arrays for Ka-band 5G applications," *IEEE Antennas Wireless Propag. Lett.*, vol. 20, pp. 2038–2042, 2021.

[9] Y. He, S. Lv, L. Zhao, G. L. Huang, X. Chen, and W. Lin, "A compact dual-band and dual-polarized millimeter-wave beam scanning antenna array for 5G mobile terminals," *IEEE Access*, vol. 9, pp. 109042–109052, 2021.

[10] S. J. Yang, S. F. Yao, R. Y. Ma, and X. Y. Zhang, "Low-profile dual-wideband dual-polarized antenna for 5G millimeter-wave communications," *IEEE Antennas Wireless Propag. Lett.*, vol. 21, pp. 2367–2371, 2022.

[11] M. Wang and C. H. Chan, "Dual-polarized, low-profile dipole-patch array for wide bandwidth applications," *IEEE Trans. Antennas Propag.*, vol. 70, no. 9, pp. 8030–8039, Sep. 2022.

[12] X. Dai and K. M. Luk, "A wideband dual-polarized antenna for millimeter-wave applications," *IEEE Trans. Antennas Propag.*, vol. 69, no. 4, pp. 2380–2385, Apr. 2021.

[13] F. F. Fan, Q. L. Chen, Y. X. Xu, X. F. Zhao, J. C. Feng, and Z. H. Yan, "A wideband compact printed dipole antenna array with SICL feeding network for 5G application," *IEEE Antennas Wireless Propag. Lett.*, vol. 22, pp. 283–287, 2023.

[14] J. Xu, W. Hong, Z. H. Jiang, and H. Zhang, "Millimeter-wave broadband substrate integrated magneto-electric dipole arrays with corporate low-profile microstrip feeding structures," *IEEE Trans. Antennas Propag.*, vol. 68, no. 10, pp. 7056–7067, Oct. 2020.

[15] J. Sun, A. Li, and K. M. Luk, "A high-gain millimeter-wave magneto-electric dipole array with packaged microstrip line feed network," *IEEE Antennas Wireless Propag. Lett.*, vol. 19, pp. 1669–1673, 2020.

[16] X. Dai, A. Li, and K. M. Luk, "A wideband compact magneto-electric dipole antenna fed by SICL for millimeter wave applications," *IEEE Trans. Antennas Propag.*, vol. 69, no. 9, pp. 5278–5285, Sep. 2021.

[17] J. Xu, K. M. Luk, and W. Hong, "Low-profile wideband circularly polarized complementary antenna and arrays for millimeter-wave communications," *IEEE Trans. Antennas Propag*, vol. 71, no. 3, pp. 2052–2063, Mar. 2023.

[18] J. Xu, X. Xia, K. M. Luk, and W. Hong, "Millimeter-wave array antennas using broadband 3D folded strip elements for B5G/6G communications," *IEEE Trans. Antennas Propag.*, vol. 70, no. 12, pp. 11569–11581, Dec. 2022.

[19] E. Baldazzi et al., "A high-gain dielectric resonator antenna with plastic-based conical horn for millimeter-wave applications," *IEEE Antennas Wireless Propag. Lett.*, vol. 19, pp. 949–953, 2020.

[20] J. Kowalewski, J. Eisenbeis, A. Jauch, J. Mayer, M. Kretschmann, and T. Zwick, "A mmW broadband dual-polarized dielectric resonator antenna based on hybrid modes," *IEEE Antennas Wireless Propag. Lett.*, vol. 19, pp. 1068–1072, 2020.

[21] Y. Zhang, J. Y. Deng, M. J. Li, D. Sun, and L. X. Guo, "A MIMO dielectric resonator antenna with improved isolation for 5G millimeter-wave applications," *IEEE Antennas Wireless Propag. Lett.*, vol. 18, pp. 747–751, 2019.

[22] Y. M. Pan, X. Qin, Y. X. Sun, and S. Y. Zheng, "A simple decoupling method for 5G millimeter-wave MIMO dielectric resonator antennas," *IEEE Trans. Antennas Propag.*, vol. 67, no. 4, pp. 2224–2234, Apr. 2019.

[23] C. Ma, S. Y. Zheng, Y. M. Pan, and Z. Chen, "Millimeter-wave fully integrated dielectric resonator antenna and its multi-beam application," *IEEE Trans. Antennas Propag.*, vol. 70, no. 8, pp. 6571–6580, Aug. 2022.

[24] H. Li, Y. Cheng, L. Mei, and L. Guo, "Frame integrated wideband dual-polarized arrays for millimeter-wave/sub 6-GHz mobile handsets and its user effects," *IEEE Tran. Veh. Technol.*, vol. 69, no. 12, pp. 14330–14340, Dec. 2020.

[25] Y.-T. Liu et al., "1-D wideband phased dielectric resonator antenna array with improved radiation performance using characteristic mode analysis," *IEEE Trans. Antennas Propag.*, vol. 71, no. 7, pp. 6179–6184, Jul. 2023.

[26] Y. T. Liu, B. Ma, S. Huang, S. Wang, Z. J. Hou, and W. Wu, "Wideband low-profile connected rectangular ring dielectric resonator antenna array for millimeter-wave applications," *IEEE Trans. Antennas Propag.*, vol. 71, no. 1, pp. 999–1004, Jan. 2023.

[27] L. X. Cui, X. H. Ding, W. W. Yang, L. Guo, L. H. Zhou, and J. X. Chen, "Communication compact dual-band hybrid dielectric resonator antenna for 5G millimeter-wave applications," *IEEE Trans. Antennas Propag.*, vol. 71, no. 1, pp. 1005–1010, Jan. 2023.

[28] Z. Chen et al., "Millimeter-wave rectangular dielectric resonator antenna array with enlarged DRA dimensions, wideband capability, and high-gain performance," *IEEE Trans. Antennas Propag.*, vol. 68, no. 4, pp. 3271–3276, Apr. 2020.

[29] I. A. Zubir et al., "A low-profile hybrid multi-permittivity dielectric resonator antenna with perforated structure for Ku and K band applications," *IEEE Access*, vol. 8, pp. 151219–151228, 2020.

[30] Y. Li and K. M. Luk, "Wideband perforated dense dielectric patch antenna array for millimeter-wave applications," *IEEE Trans. Antennas Propag*, vol. 63, no. 8, pp. 3780–3786, Aug. 2015.

[31] A. A. Qureshi, D. M. Klymyshyn, M. Tayfeh, W. Mazhar, M. Börner, and J. Mohr, "Template-based dielectric resonator antenna arrays for millimeter-wave applications," *IEEE Trans. Antennas Propag.*, vol. 65, no. 9, pp. 4576–4584, Sep. 2017.

[32] Y. Li and K. M. Luk, "A 60-GHz dense dielectric patch antenna array," *IEEE Trans. Antennas Propag.*, vol. 62, no. 2, pp. 960–963, Feb. 2014.

[33] H. Chu and Y. X. Guo, "A novel approach for millimeter-wave dielectric resonator antenna array designs by using the substrate integrated technology," *IEEE Trans. Antennas Propag.*, vol. 65, no. 2, pp. 909–914, Feb. 2017.

[34] K. Gong and X. H. Hu, "Low-profile substrate integrated dielectric resonator antenna implemented with PCB process," *IEEE Antennas Wireless Propag. Lett.*, vol. 13, pp. 1023–1026, 2014.

JIE-ER ZHANG was born in Nantong, Jiangsu, China, in 1999. He received the B.S. degree in electronic science and technology from Nantong University Xinglin College, Nantong, in 2021. He is currently pursuing the M.S. degree with the School of Materials Science and Engineering, Yancheng Institute of Technology. His current research interest is microwave antenna.

QINFANG ZHANG was born in Danyang, Jiangsu, China, in 1980. He received the B.S. degree from Xuzhou Normal University, Xuzhou, Jiangsu, China, in 2000, and the M.S. and Ph.D. degrees from Nanjing University, Nanjing, China, in 2005. Since 2012, he has been with the Yancheng Institute of Technology, Yancheng, Jiangsu, China, where he is currently a Professor. He has authored or coauthored more than 100 internationally referred journal and conference papers. He holds 19 Chinese patents and one U.S. patent. His research interests include development and application of cluster beam deposition technology and materials informatics.

WEI QIN (Member, IEEE) was born in Jiangsu, China. He received the B.Sc. degree in electronic engineering and the M.Sc. degree in electromagnetic fields and microwave technology from Southeast University, Nanjing, China, in 2007 and 2010, respectively, and the Ph.D. degree in electronic engineering from the City University of Hong Kong, Hong Kong, China, in 2013.

From July 2013 to November 2013, he was a Senior Research Associate with the State Key Laboratory of Millimeter Waves, City University of Hong Kong. Since 2014, he has been with the School of Electronics and Information, Nantong University, Nantong, Jiangsu, where he is currently a Professor. His research interests include deign and application of microwave devices and antennas.

WEN-WEN YANG (Member, IEEE) received the B.Eng. degree in information engineering and the M.Eng. and Ph.D. degrees in electrical engineering from Southeast University, Nanjing, China, in 2007, 2010, and 2015, respectively.

Since 2015, he has been with the School of Electronics and Information, Nantong University, Nantong, China, where he is currently an Associate Professor. From August 2018 to August 2019, he was a Visiting Researcher with Polytechnique Montréal, Montreal, Canada. He has authored or coauthored more than 50 internationally referred journal and conference papers. His research interests include RF, microwave and millimeter-wave passive devices, active antenna array, and antennas for wireless communication. He serves as a reviewer for several IEEE and IET journals.

JIAN-XIN CHEN (Senior Member, IEEE) was born in Nantong, Jiangsu, China, in 1979. He received the B.S. degree from Huaiyin Teachers College, Huaiyin, Jiangsu, China, in 2001, the M.S. degree from the University of Electronic Science and Technology of China, Chengdu, China, in 2004, and the Ph.D. degree from the City University of Hong Kong, Hong Kong, in 2008.

Since 2009, he has been with Nantong University, Nantong, where he is currently a Professor. He has authored or coauthored more than 100 internationally referred journal and conference papers. He holds 25 Chinese patents and three U.S. patents. His research interests include microwave active/passive circuits and antennas, LTCC-based microwave and millimeter-wave filters and devices, and dielectric resonator filters and antennas. He was a recipient of the New Century Excellent Talents in University of the Ministry of Education for China in 2011. He was a supervisor of several conference best paper award winners.